NOVEL FEATURES OF THE HELICAL VOLUMETRIC NEUTRON SOURCE FFHR-b2

J. Miyazawa[1,2], T. Goto[1,2], Y. Hamaji[1,2], M.I. Kobayashi[1,2]

[1] National Institute for Fusion Science (NIFS), Toki, Gifu, 509-5292, Japan
[2] The Graduate University for Advanced Studies, Toki, Gifu, 509-5292, Japan

E-mail:miyazawa.junichi@nifs.ac.jp

Received xxxxxx
Accepted for publication xxxxxx
Published xxxxxx

Abstract

The compact helical fusion reactor FFHR-b2 is a multipurpose HElical Volumetric Neutron Source (HEVNS) available as the component test facility to test the divertor and blanket systems. In the latest design, three new technologies of the HTS (High-Temperature Superconducting) conductor, the ceramic pebble divertor, and the cartridge-type blanket are adopted. Tin-based functional liquid metals (FLMs) including lithium are considered as the working fluid for the blanket. The FLMs have multi functions of low vapor pressure, low density, low melting point, low corrosiveness, high tritium breeding ratio, and so on. The target construction cost of the FFHR-b2 has been set to 200 billion JPY. The main target of FFHR-b2 is to demonstrate the fusion gain larger than one. To achieve this in a relatively small device, the tangential Neutral Beam Injection (NBI) heating with a moderate energy of 80 keV is adopted for the FFHR-b2. The beam-plasma fusion with 5 MW of NBI heating can produce a fusion power of 5 MW that is larger than the absorbed power of 3 MW.

Keywords: fusion reactor, neutron source, divertor, blanket, liquid metal

1. Introduction

Because of the largest fusion reaction cross section between deuterium (D) and tritium (T) atoms [1], DT fusion is considered to be the main reaction in conservative fusion reactors. Neutrons produced by the DT fusion reaction have a high energy of 14 MeV and severely damage materials of fusion reactor components. On the other hand, the neutrons which are free from the magnetic field can be easily captured by a device called the blanket surrounding the plasma. Lithium (Li) atoms stocked inside the blanket are hit and broken by the neutrons and produces T and helium (He) atoms. The number called TBR (Tritium Breeding Ratio) is the ratio of the total number of T atoms generated in the blanket to the total number of 14 MeV neutrons produced in the plasma, which is equal to the number of DT fusion reactions occurred in the plasma. The TBR should be larger than one to sustain the fusion reactor without supplying T other than the initial loading. Before building a fusion reactor, two kinds of neutron sources are highly needed. One is for material test, and another is for component test of the blanket. In both cases, steady-state operation for longer than a few months is the common requirement. For the material test, the intensity of neutron flux has a priority over the neutron irradiation area. A high neutron flux of the order of 10^{18} – 10^{19} n/m^2/s is needed to carry out the neutron irradiation tests of 10 dpa/year. Beam-target neutron sources of A-FNS and DONES have been designed for the neutron irradiation test in Japan and Europe, respectively, after the long discussion on IFMIF/EVEDA [2]. On the other hand, the priority of the neutron source for component test should be placed on the neutron irradiation area, which can cover a large plasma facing surface of the blanket. Otherwise, it is impossible to check if the blanket can achieve TBR > 1 or not. From this point of view, the neutron source as the Component Test Facility (CTF) should have the same geometry with the supposed fusion reactor, even if the device size is proportionally reduced to save the construction

cost. A pilot plant that works as a CTF enabling Fusion Nuclear Science and Technology (FNST) research has been discussed in US [3].

Design studies on the helical fusion reactors, which are called the FFHR series, has been conducted since 1994 [4,5]. The FFHR series are designed based on the knowledges on plasma physics and fusion engineering obtained through construction and operation of the LHD (Large Helical Device) [6]. The LHD is a superconducting device equipped with two helical coils and six circular coils. A helical plasma can be confined in the magnetic field generated by these superconducting magnet coils. Since no plasma current is required, it is easier to sustain a high-temperature plasma in steady state, compared with tokamaks. The helical plasma is quietly generated at a fixed position in the vacuum vessel (VV) and never hit the VV wall at the start-up and/or shut-down phases. No disruptive event related to the plasma current is expected for the helical plasma. The FFHR design group has proposed a step-by-step approach starting from a small device toward a large costly fusion reactor [7], *i.e.*, starting from a small cold test device named FFHR-a1, through FFHR-b1 and FFHR-c1, toward FFHR-d1. The FFHR-b1 has been updated to FFHR-b2 and FFHR-b3. The updated device parameters are listed in Table. 1, where R_c is the helical coil major radius, B_c is the magnetic field strength at R_c, P_{aux} is the auxiliary heating power, P_{fusion} is the fusion output, C_{direct} is the direct cost, and τ_{life} is the device lifetime at full power operation, determined by the maximum neutron fluence of 10^{23} n/m^2 on the helical coil. These parameters are estimated by the system code HELIOSCOPE [8]. The main target of the FFHR-b2 is to demonstrate $Q_{eff} \equiv P_{fusion} / P_{abs} > 1$, where P_{abs} is the auxiliary heating power absorbed by the plasma. On the other hand, the main target of the FFHR-b3 is to demonstrate the net electricity generation larger than the total electric power used to operate the device, with a reasonable R_c, B_c, and C_{device}. To achieve $Q_{eff} = 1$ in a small device, the tangential Neutral Ion Beam injection (NBI) heating is adopted in the FFHR-b2, while the Electron Cyclotron Heating (ECH) is the main heating method in the FFHR-b3. This manuscript focuses on the FFHR-b2, which can be used as the HElical Volumetric Neutron Source (HEVNS) with a reasonable device size. Main features of the FFHR-b2 are described in Section 2. Expected plasma parameters and neutron fluxes are discussed in Section 3. These are summarized in Section 4.

2. Main Features of the FFHR-b2

In the latest design of FFHR-b2, several points have been changed from the former FFHR-b1 design: (1) The device size is 1.4 times increased from R_c = 3.90 m to R_c = 5.46 m to enlarge the blanket space and prolong the τ_{life}, (2) The B_c is reduced from 5.7 T to 5.46 T, (3) The helical coil pitch parameter, α, is changed from 0.1 as in the LHD to 0.0, to simultaneously improve the MHD stability and the neoclassical transport [9], (4) the magnets are basically consisted of the HTS (High-Temperature Superconducting) NI-WISE (No Insulation, Wound and Impregnated Stacked Elastic tapes) conductor [10] and cooled by liquid hydrogen of ~20 K, (5) the tungsten helical divertor and the ceramic pebble divertor named the REVOLVER-D3 (Reactor-oriented Effectively VOLumetric VERtical Divertor, the 3rd version) are adopted in parallel, (6) the CARDISTRY-B2 (CARtridges Divided and InSerTed RadiallY – Blanket, the 2nd version) [11] is adopted for the blanket, and (7) austenitic stainless steels are basically chosen as the main structure materials, instead of the RAFM (Reduced Activation Ferritic/Martensitic) steels, to reduce C_{direct}. A schematic view of the FFHR-b2 is depicted in Fig. 1. Two pairs of tangential NBI systems are installed in the FFHR-b2. The balanced injection not to drive a large plasma current will be supplyed by each pair including co and counter directed NBI. The two pairs will be used alternately in long-pulse operations.

Table 1. List of the updated device parameters of the FFHR series.

	FFHR-a1	FFHR-b1	FFHR-b2	FFHR-b3
R_c (m)	2.73	3.90	5.46	7.80
B_c (T)	4.0	5.7	5.33	6.6
P_{aux} (MW)	5	5	5	30
P_{fusion} (MW)	0	~5	~5	~340
C_{direct} (10^8 JPY)	~510	~1,200	~2,000	~5,700
τ_{life} (years)	-	~0.36	~2.7	~5.0

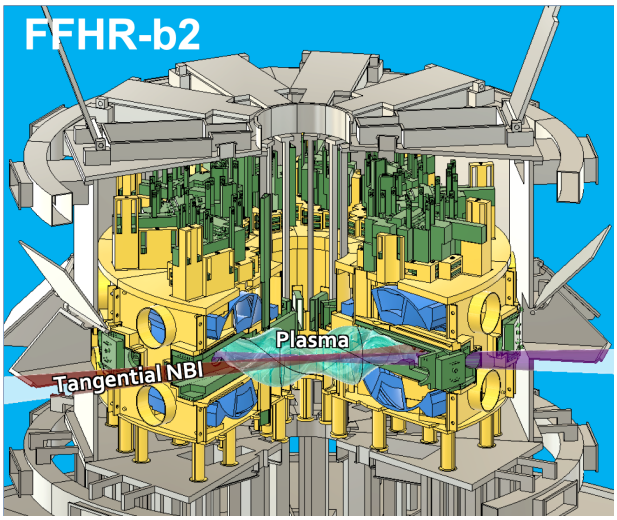

Figure 1. Beam Energy multiplication factor as a function of ion temperature in the case of the beam acceleration energy of 100 keV.

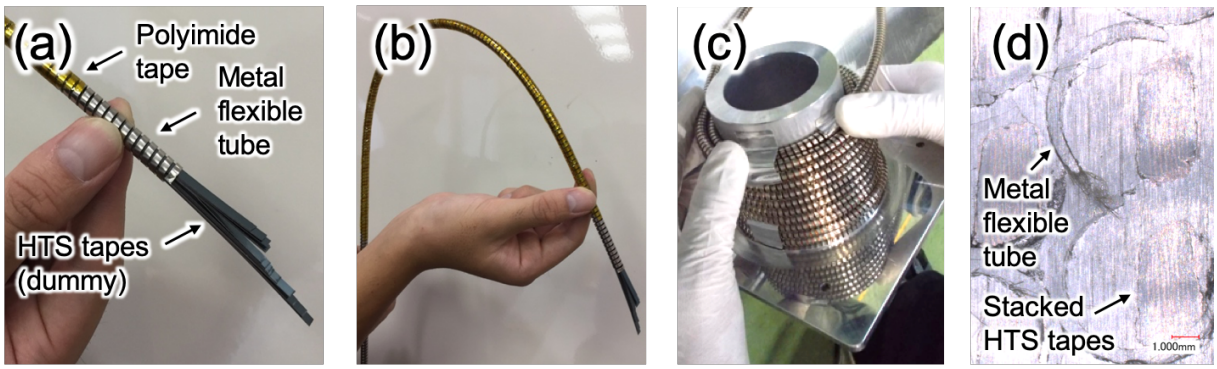

Figure 2. (a) A close-up view of the WISE conductor, (b) flexibility of the WISE conductor, (c) a small solenoid coil wound with the WISE conductor without insulation, and (d) a close-up view of the cross section of the solenoid coil sliced after impregnation with low melting point metal.

The WISE conductor is a new conductor, where simply stacked HTS tapes are bundled inside a metal flexible tube [10], as shown in Fig. 2. Because of its high flexibility, it is quite easy to wind the helical coils. After the coil winding process is completed, the coil is heated up to ~100℃ and impregnated by a low melting temperature alloy as the U-Alloy78 ($Bi_{57}Sn_{17}In_{26}$, melting point ~78.8℃). In Figs. 2(a) and 2(b), polyimide tape is wound around the metal flexible tube for insulation. It is possible to use the WISE conductor without insulation, *i.e.*, as the NI-WISE conductor, as shown in Figs. 2(c) and 2(d). Both heat conductivity and heat capacity of the conductor can be increased if insulation is omitted, although the current rise time will increase. Even if a transition to normal conducting state takes place in the coil, the electric current in the normal region immediately bypasses to the neighbouring superconducting tapes. Then, no Joule heating continues in the normal region. As long as an enough cooling power is supplied, the normal region can recover to the superconducting state. This works as the powerful quench protection scenario for the coils wound with the NI-WISE conductor.

The REVOLVER-D3 is a newly proposed limiter/divertor system using falling massive ceramic pebbles as the Plasma Facing Material (PFM). This concept is based on the former concepts of the REVOLVER-D [12] and the REVOLVER-D2 [13,14], which adopt the melted tin shower jets and the solid tin pebbles, respectively, for the PFM. The multi-layered ceramic pebble divertor concept was intensively studied in Osaka Univ. in the early 2000s [15-18]. The cascading pebble divertor using W-coated SiC pebbles or W-coated graphite pebbles was adopted in the conceptual design of an STPP (Spherical Tokamak Power Plant) [19] and an ST-based CTF [20]. More recently, the ferromagnetic pebble divertor concept was proposed by the FZJ group [21]. Our proposal can be distinguished from these former studies in that the REVOLVER-D3 will employ pure ceramic pebbles of SiC or other. A conceptual diagram of the REVOLVER-D3 is depicted in Fig. 3. In the FFHR-b2, ten modules are installed

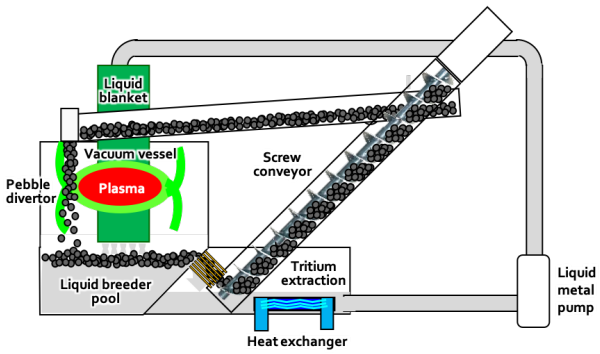

Figure 3. A conceptual diagram of the ceramic pebble divertor REVOLVER-D3.

near the inner ports to inject the ceramic pebbles through the ergodic layer surrounding the main plasma. The ceramic pebble flow plays a role of the limiter inserted to the ergodic layer. The plasma flowing out from inside of the LCFS (Last Closed Flux Surface) turns toroidally in the ergodic layer for at least a few times before reaching the divertor. During this stagnation, a significant portion of the outflowing plasma hits the pebble flow and becomes recombined. According to the simulation results, roughly 70 % of the outflowing plasma can be captured by the pebble flow [22]. The rest 30 % goes to the helical divertor region covered by W target plates. The ceramic pebbles fall into a pool filled with melted metals exhausted from the blanket cartridges. The dropping impact of the massive ceramic pebbles is absorbed by the melted metal. The ceramic pebbles heated by the plasma is cooled in the melted metal pool. After the filtering process, the ceramic pebbles are separated from the meted metal and vertically transported by screw conveyers. Then, the ceramic pebbles are dropped to the ergodic layer again to repeat the circulation process.

The CARDISTRY-B2 is an improved version of the cartridge-type helical blanket system, where the total number of cartridges are roughly halved, tangential ports for the effective tangential NBI heating are newly equipped, and the

compatibility with the helical divertor is considered [11]. The maintainability has been also improved. The construction and maintenance schemes using the combination of high-power crane robots and dexterous (but low-power) robots are now being considered with small 3D-printed models and robots. As shown in Fig. 4, the liquid metal flows inside the blanket cartridges and then exhausted to the pool inside the plasma vacuum vessel. Since the free surface of the liquid metal is exposed to the plasma, the vapor pressure of the liquid metal should be low enough not to deteriorate the plasma performance. The pebbles from the REVOLVER-D3 system also flow into the liquid metal pool.

The liquid metal to be used in the CARDISTRY-B2 should satisfy several requirements of low vapor pressure, low density, low melting point, low corrosiveness, high TBR, and high neutron shielding ability. Especially, the vapor pressure at the working temperature of ~500℃ should be low enough, since the free surface of the liquid metal filled in the pool is exposed to the plasma. To satisfy these requirements, ternary or quaternary alloys, which include Li, Sn, Pb (or Bi), and Er, are selected as the candidates of the Functional Liquid Metal (FLM). Six candidates of $Pb_{74.8}Li_{25}Er_{0.2}$ (PLE-25), $Bi_{74.8}Li_{25}Er_{0.2}$ (BLE-25), $Sn_{74.8}Li_{25}Er_{0.2}$ (SLE-25), $Sn_{68.8}Li_{25}Pb_6Er_{0.2}$ (SLPE-25), and $Sn_{43.3}Bi_{31.5}Li_{25}Er_{0.2}$ (SBLE-25) have been selected to date. The names in parentheses are abbreviation for the initials of the materials included, listed in descending order of atomic ratio, and the numbers denote the atomic ratio (at%) of Li. Tin has very low vapor pressure [23], and therefore, has been chosen as the base material except for PLE-25 and BLE-25. For example, the vapor pressures at a working temperature of 500℃ of PLE-25, SLE-25, and SLPE-25, and SBLE-25 are 1.4×10^{-3} Pa, 1.8×10^{-5} Pa, and 8.4×10^{-5} Pa, respectively. These are estimated by taking the chemical activities of the compositions [23] into account. The vapor pressures of SLE-25 and SLPE-25, which include tin as the main composition, are lower than that of PLE-25, which includes no tin. Lithium is necessary to produce tritium through a spallation reaction. For comparison, the atomic composition of Li is fixed to 25 % in all candidate FLMs. Lead is added to tin to decrease the melting point and at the same time, to mitigate the corrosiveness of tin. Bismuth is selected as the substituting material for lead, to avoid troublesome handling of lead in basic experiments. A small amount of erbium is added expecting self-formation and/or self-recovery of the oxidized erbium layer that works as an anticorrosion film on the blanket materials. The attempt to form an oxidized erbium layer on vanadium alloys by adding a small amount of erbium in liquid lithium was successfully done in the past studies [24-26]. However, it has not been confirmed yet if this works for the different combinations of liquid metals and materials. Further research on this is highly required. In our case, erbium is chosen as the oxidizing substances as in Refs. 24-26, since erbium has much lower oxygen potential than lithium [27]. Basic experiments on the FLM is now ongoing.

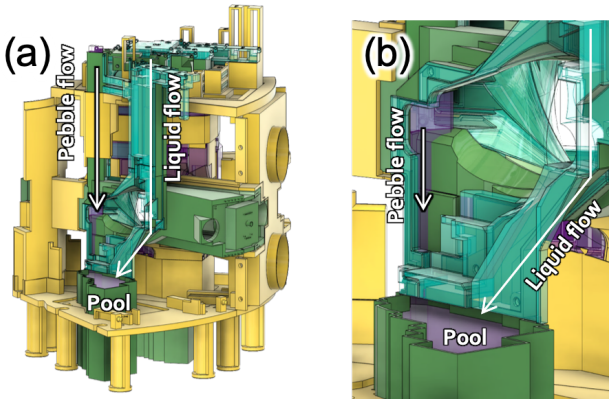

Figure 4. (a) A schematic view and (b) a close-up view of the CARDISTRY-B2.

3. Expected Performance of the FFHR-b2

The FFHR-b2 is basically a beam-plasma fusion reactor, where 80 keV - 5 MW tangential D beam is injected to the target DT plasma, of which the T ratio is changed from 0 to 100 %. The fusion output is estimated by an iterative calculation as follows; (1) determine the ion and electron temperature profiles by the DPE (Direct Profile Extrapolation) method [28-31] using assumed ion and electron density profiles and a heat deposition profile of NBI, (2) calculate the magnetic equilibrium by the VMEC code [32] using the pressure profiles obtained, (3) calculate the NBI heat deposition profile and the birth profile of alpha particles generated by the beam-plasma fusion reaction by the FIT3D code [33] using the magnetic equilibrium, (4) return to (1) and recalculate the temperature profiles, and then repeat the procedure from (1) to (4) until the temperature profiles converge, (5) recalculate the heat deposition and pressure profiles of NBI and alpha particles by the GNET code [34-36] using the converged temperature profiles, (6) return to (1) and recalculate the temperature profiles, and then repeat the procedure from (1) to (6) until the temperature profiles and magnetic equilibrium converge. In this study, the last iteration was not necessary because the magnetic equilibrium obtained using the GNET results were already well converged.

In this study, an assumed confinement improvement factor, H, of 1.3 and a confinement degradation factor, f_{deg}, due to the Shafranov shift of the magnetic axis were multiplied to a scaling factor, f_τ, of the energy confinement time, τ_E, in the DPE method [28-31]. The H = 1.3 is assumed because the optimized magnetic configuration with α = 0.0 is adopted in the FFHR-b2, as discussed in the former section. The reference profiles used in this study was taken from a hydrogen discharge. Confinement improvement due to the isotope effect as reported in the LHD experiments [37-39] is

also included in H = 1.3. It is necessary to confirm these improvement effects in the experiments. This should be done in the FFHR-a1, which is the smaller version of the FFHR-b2. On the other hand, f_{deg} is also newly introduced to the DPE method in this study. In LHD, it has been reported that the τ_E depends on the magnetic configuration. In the inward-shifted configurations, where the magnetic axis, R_{ax}, is smaller than the major radius of the helical coil, R_c, the τ_E tends to be larger than those in the outward-shifted configurations with $R_{ax} \sim R_c$. This effect was considered with a renormalization factor, f_{ren}, when the helical/stellarator energy confinement time scaling, ISS95 [40], was updated to ISS04 [41]. The f_{ren} for the LHD data can be fitted as below,

$$f_{ren}(R_{ax} / R_c) = 0.483\ (R_{ax} / R_c)^{-8.26}, \quad (1)$$

where R_{ax} is the major radius of the magnetic axis and R_c is the major radius of the helical coil. In the case of LHD, where R_c =3.90 m, Eq. (1) can be applicable in the range of 3.60 m < R_{ax} < 3.90 m, or, 0.923 < (R_{ax} / R_c) < 1.0.

To estimate a typical fusion output in the FFHR-b2, the DPE method has been applied on the radial profile data obtained in the LHD experiment. The reference profiles adopted in this study are those at the time of t = 3.533 s in the shot #115772, where a hydrogen plasma was heated by the tangential hydrogen NBI. The same profiles are also used in Ref. 9. The magnetic configuration in the shot was R_{vac} = 3.55 m, where R_{vac} is the major radius of the magnetic axis in vacuum. The central beta, β_0, and R_{ax} at t = 3.533 s were ~2.4 % and ~3.69 m, respectively. If the β_0 estimated in the DPE method is higher than 2.4 %, (R_{ax} / R_c) becomes larger than (3.69 / 3.90) due to the Shafranov shift and this will cause a confinement degradation as expressed in Eq. (1). To take this effect into account, the confinement degradation factor, f_{deg}, derived from Eq. (1) as below, was multiplied to f_t, together with H.

$$f_{deg}(R_{ax} / R_c) = 0.636\ (R_{ax} / R_c)^{-8.26}, \quad (2)$$

where R_c = 5.46 m in FFHR-b2 discussed in this study. Note that f_{deg} becomes larger than unity, if β_0 is lower than 2.4 % and (R_{ax} / R_c) < (3.69 / 3.90).

Calculation results of the fusion output in FFHR-b2, where a 100 % T plasma is heated by the tangential D NBI with a fixed heating power, P_{NB}, of 5 MW, are summarized in Fig. 5. In the figure, β_0, P_{fusion}, P_{abs}, and Q are plotted with respect to the central electron density, n_{e0}, for two cases with H = 1.0 and 1.3. As seen in Fig. 5(a), β_0 is as high as ~1.5 % at the low-density range of n_{e0} < 0.6 × 10^{19} m^{-3} and decreases to ~0.8 % as the density increases to 3 × 10^{19} m^{-3}. This seems strange, since it is ordinary observed that β_0 increases with n_{e0}, following the gyro-Bohm model where the plasma pressure is proportional to the 0.6 power of the density [30,42]. This

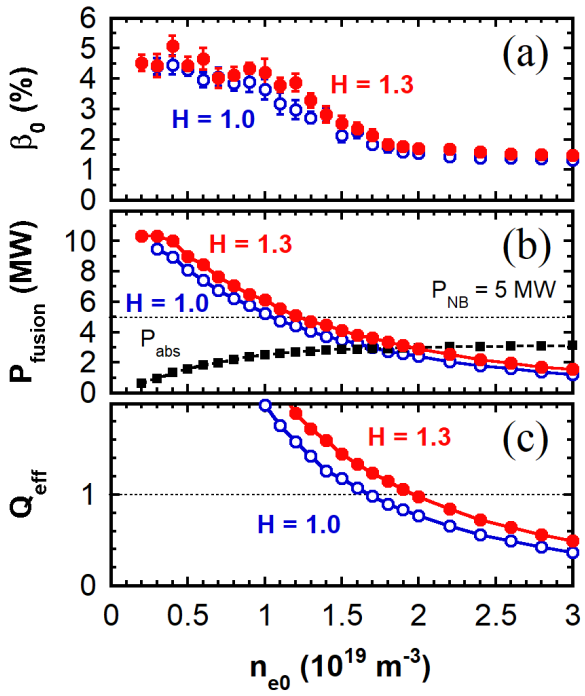

Figure 5. Calculation results of the DPE method for FFHR-b2, where (a) β_0, (b) P_{fusion} and P_{abs}, and (c) Q_{eff}, are plotted with respect to n_{e0}. Open and Closed circles denote H = 1.0 and 1.3, respectively.

strange behavior is due to the pressures of high-energy beam ions and alpha particles. Indeed, the beta of the bulk plasma is smaller than 0.2 % at n_{e0} < 1 × 10^{19} m^{-3}. As was discussed above, the Shafranov shift larger than that in the reference data can cause the confinement degradation. In the case of Fig. 5, however, β_0 is lower than 2.4 % of the reference data. As a result, (R_{ax} / R_c) is within the range from 0.923 to 0.938 and f_{deg} is within the range from 1.08 to 1.23, which is larger than unity, according to Eq. (2).

It should be noted that P_{abs} < P_{NB} at low-density, as shown in Fig. 5. Both the charge-exchange reaction and the ion-impact ionization between the high-energy neutral beams and the main plasma decreases as the density decreases. As a result, a large amount of beam neutrals passes through the main plasma at low-density. This "shine-through" effect saturates at n_{e0} > 2 × 10^{19} m^{-3}, and P_{abs} saturates to ~3 MW. However, this P_{abs} is still smaller than P_{NB} = 5 MW. This is due to the orbit loss. A part of beam ions deposited at the edge region of the main plasma can be immediately lost, since a high-energy beam ion having a large Larmor radius traces a large orbit and deviates from the confinement region.

The P_{fusion} calculated by taking the f_{deg} into account for the case with H = 1.3 is larger than P_{abs}, and therefore Q_{eff} is larger than one, at n_{e0} < 1.7 × 10^{19} m^{-3}, as shown in Figs. 5(b) and 5(c), respectively. Even in the case with H = 1.0, Q_{eff} > 1 can be achieved at n_{e0} < 1.4 × 10^{19} m^{-3}. The typical operation of

FFHR-b2 with P_{NB} = 5 MW will be done at $n_{e0} \sim 1 \times 10^{19}$ m^{-3}, where $P_{fusion} \sim 5$ MW with $H = 1.0 - 1.3$, *i.e.*, $Q \equiv P_{fusion} / P_{NB} \sim 1$. Then, 14 MeV neutrons of 4 MW in total can be produced. This corresponds to ~1.8×10^{18} n/s of neutron production rate. Assuming that the neutrons irradiate a toroidal surface of ~130 m^2, with 5.46 m of major radius and 0.85 m of minor radius, which corresponds to the minimum distance from the plasma center to the inboard side blanket surface, then the neutron flux is ~0.022 MW/m^2 ~ 8×10^{15} n/m^2/s. Although this neutron flux is 10^2 – 10^3 times smaller than that required for the neutron sources for material test, it is large enough to test the functions of the blanket. Due to the small devise size of the FFHR-b2 and the resultant blanket thickness, the neutron shielding performance of the blanket is not necessarily enough for the superconducting helical coils. According to the estimation by the HELIOSCOPE, the τ_{life} at the full power operation is as short as ~2.7 years, as was listed in Table 1. However, from the point of view of the component test of the helical coil, it is favorable if one can accomplish the life evaluation test within a few years.

4. Summary

The FFHR-b2, of which the device size is 1.4 times larger and the magnetic field is ~ 2 times larger than those of the LHD, is an optional device defined in the development strategy toward realization of the helical fusion reactor. The main mission of the FFHR-b2 is to comprehensively demonstrate the technology readiness of the new technologies on the HTS magnets (NI-WISE conductor), the ceramic pebble divertor (REVOLVER-D3), and the cartridge-type liquid metal blanket (CARDISTRY-B2) adopting the FLM as the working fluid, under a real reactor condition. At the same time, FFHR-b2 must show the usefulness as the HEVNS that can supply a steady-state (year-long) neutron flux in a wide area that is enough to test the performance of the blanket. The NBI heating is adopted in the FFHR-b2 to produce a large number of neutrons in a relatively small device. According to the estimation based on the DPE method, 80 keV - 5 MW of the fusion output and ~0.022 MW/m^2 ~ 8×10^{15} n/m^2/s of the 14 MeV neutron flux will be achieved with the NBI heating of 5 MW. Although the neutron flux is 10^2 – 10^3 times smaller than that required for the material test, it is enough for the component tests to clarify the TBR of the blanket, the performance of the divertor, the life of the superconducting magnets, and so on. To promote the commercial use of the FFHR-b2, the construction cost of ~200 billion JPY, or lower, must be also proven.

Acknowledgements

The authors wish to thank Prof. S. Murakami and Mr. Y. Shoji of Kyoto University for their help in estimating heat deposition and pressure profiles of NBI and alpha particles by the GNET code. The authors also thank all the members of the FFHR design group for fruitful discussions and comments on the manuscript. This work was supported by the budgets of NIFS15UFFF038 and NIFS17UFFF040 of the National Institute for Fusion Science.

References

[1] For example, W.A. Fowler, G.R. Caughlan, and B.A. Zimmerman, Ann. Astron. Astrophys. **13**, 69 (1975).
[2] J. Knaster et al., Nucl. Mater. Energy **9** (2016) 46.
[3] J.E. Menard et al., Nucl. Fusion **51** (2011) 103014.
[4] A. Sagara et al., Fusion Eng. Des. **29** (1995) 51.
[5] A. Sagara et al., Nucl. Fusion **57** (2017) 086046.
[6] A. Komori et al., Fusion Sci. Technol. **58** (2010) 1.
[7] J. Miyazawa et al., Fusion Eng. Des. **146** (2019) 2233.
[8] T. Goto et al., Nucl. Fusion **51** (2011) 083045.
[9] T. Goto et al., Nucl. Fusion **59** (2019) 076030.
[10] S. Matsunaga et al., IEEE Trans. Appl. Supercond. **30** (2020) 4601405.
[11] J. Miyazawa et al., Plasma Fusion Res. **14** (2019) 1405163.
[12] J. Miyazawa et al., Fusion Eng. Des. **125** (2017) 227.
[13] T. Ohgo et al., Plasma Fusion Res. **14** (2019) 3405050.
[14] T. Ohgo et al., Fusion Eng. Des. **165** (2021) 112236.
[15] M. Isobe et al., Nucl. Fusion **40** (2000) 327.
[16] K. Matsumoto et al., Nucl. Fusion **41** (2001) 827.
[17] T. Okui et al., Fusion Technol. **39** (2001) 934.
[18] T. Okui et al., Fusion Eng. Des. **61-62** (2002) 203.
[19] G. Voss et al., Fusion Eng. Des. **81** (2006) 327.
[20] G. Voss et al., Fusion Eng. Des. **83** (2008) 1648.
[21] N. Gierse et al., Nucl. Mater. Energy **2** (2015) 12.
[22] G. Kawamura et al., Plasma Fusion Res. **13** (2018) 3403034.
[23] M. Kondo and Y. Nakajima, Nucl. Fusion **88** (2013) 2556.
[24] Z. Yao et al., J. Nucl. Mater. **329-333** (2004) 1414.
[25] Z. Yao et al., Fusion Eng. Des. **81** (2006) 951.
[26] T. Chikada et al., Fusion Eng. Des. **82** (2007) 2572.
[27] M. Kondo et al., IAEA-TECDOC-1912 (2020) 157.
[28] J. Miyazawa *et al*., Fusion Eng. Des. **86** (2011) 2879.
[29] J. Miyazawa *et al*., Nucl. Fusion **52** (2012) 123007.
[30] J. Miyazawa *et al*., Nucl. Fusion **54** (2014) 013014.
[31] J. Miyazawa *et al*., Nucl. Fusion **54** (2014) 043010.
[32] S.P. Hirshman and J.C. Whitson, Phys. Fluids **26** (1983) 3553.
[33] S. Murakami, N. Nakajima, and M. Okamoto, Trans. Fusion Technol. **27** (1995) 256.
[34] S. Murakami et al., Nucl. Fusion **40** (2000) 693.
[35] S. Murakami et al., Fusion Sci. Technol. **46** (2004) 241.
[36] Y. Masaoka, and S. Murakami, Nucl. Fusion **53** (2013) 093030.
[37] H. Yamada et al., Phys. Rev. Lett. **123** (2019) 185001.
[38] K. Tanaka et al., Plasma Phys. Control. Fusion **62** (2020) 024006.
[39] T. Kobayashi et al., Nucl. Fusion **60** (2020) 076015.
[40] U. Stroth et al., Nucl. Fusion **36** (1996) 1063.
[41] H. Yamada et al., Nucl. Fusion **45** (2005) 1684.
[42] U. Stroth, Plasma Phys. Control. Fusion **40** (1998) 9.